



Published in final edited form as:

*Anal Bioanal Chem.* 2012 January ; 402(1): 325–335. doi:10.1007/s00216-011-5415-3.

## Hydrodynamic focusing – a versatile tool

Joel P. Golden, Gusphyl A. Justin, Mansoor Nasir, and Frances S. Ligler\*

Naval Research Laboratory, Center for Bio/Molecular Science and Engineering, 4555 Overlook Ave SW., Washington, DC 20375, USA

### Abstract

The control of hydrodynamic focusing in a microchannel has inspired new approaches for microfluidic mixing, separations, sensors, cell analysis and microfabrication. Achieving a flat interface between the focusing and focused fluids is dependent on Reynolds number and device geometry, and many hydrodynamic focusing systems can benefit from this understanding. For applications where a specific cross-sectional shape is desired for the focused flow, advection generated by grooved structures in the channel walls can be used to define the shape of the focused flow. Relative flow rates of the focused flow and focusing streams can be manipulated to control the cross-sectional area of the focused flows. This manuscript discusses the principles for defining the shape of the interface between the focused and focusing fluids and provides examples from our lab that use hydrodynamic focusing for impedance-based sensors, flow cytometry, and microfabrication to illustrate the breadth of opportunities for introducing new capabilities into microfluidic systems. We evaluate each example for the advantages and limitations integral to utilization of hydrodynamic focusing for that particular application.

### Keywords

hydrodynamic focusing; sheath flow; microfluidics; conductivity; flow focusing; Reynolds number

### Introduction

Two streams introduced into a straight microfluidic channel flow side-by-side down the channel as long as the fluids are matched for viscosity and hydrophobicity. In early studies, the position of one stream relative to another was manipulated in order to increase the interface between the two streams to facilitate mixing or molecular transport of molecules or particles by diffusion from one stream across the interface into the other [1–5]. However, in most of these initial studies, the flow rates of the input streams were equivalent, and hence each occupied equal volume in the channel. If one of the fluids is introduced at a higher flow rate, it occupies a larger proportion of the channel than a flow stream introduced at a lower flow rate, forcing the second stream into a smaller cross-sectional area of the channel. This process of hydrodynamic focusing has been extensively studied and used in microfluidic systems over the past ten years [5–7].

As the applications of hydrodynamic focusing expanded, the geometric manipulations of the flows became more carefully defined and the forces impacting the shape of the focused stream became better understood. Initially, it was thought that the role of inertia at low Reynolds numbers ( $Re$ ) was insignificant. Clearly, inertial forces impacted the position of one stream relative to another as the two streams passed through a Dean vortex at  $Re > 100$

\*Address for correspondence: frances.ligler@nrl.navy.mil, ph - 202-404-6002, fx - 202-767-9594.

[8]. However, we recently demonstrated unequivocally that the momentum of a focusing flow introduced into a microchannel at an angle perpendicular to the focused flow deformed the interface between the two streams at  $Re$  between 1 and 50 [9,10]. Several techniques have evolved that control the shape of the focused stream, whether to prevent unintentional deviations from a flat interface or to create a fluidic interface with a specific geometric profile. We use applications from our laboratory that implement these principles of hydrodynamic focusing for sensing, cytometry, and microfabrication of polymer materials to illustrate their relevance for design of practical microfluidic devices.

## Hydrodynamic focusing

Hydrodynamic focusing is generally envisioned as confinement or redirection of a slower flowing stream by a faster flowing stream. For the purposes of this discussion, we will not include systems intended to mix two streams together, but will direct our attention to systems where the two fluid streams function without mixing and where the channel length is sufficiently short to minimize diffusion at the  $Re$  employed. In general, the cross-sectional *area* of a focused stream can be predicted by the relative flow rates of the two streams as long as the  $Re$  and the length of the channel are consistent with minimal diffusion. However, predicting the forces that control the *shape* of the focused stream is more complex than simply calculating the ratio of the relative flow rates. In addition to the velocities at the inlets, the geometry of the microfluidic device has a major impact on the shape of the focused stream.

Due to the no-slip condition at the wall, both the focusing and focused streams have a parabolic velocity profile as they enter the main microfluidic channel. The focusing flow has a higher flow velocity in many conventional microfluidic geometries and may push the focused stream into the areas of lower pressure, i.e. corners of the channel wall. The flow profile of the focused stream consequently develops a cusped or “U” shape (Figure 1). Any increase in flow-rate ratio only exaggerates this effect, eventually splitting the focused stream into two separate streams. While in some devices, this splitting may be desirable, for many applications such as the impedance-based sensors described below, cusping of the focused conducting stream would severely reduce the sensitivity. In a different scenario, one could imagine that the intent to focus a target to a sensing surface would be confounded by cusping; in this situation, the target would be pushed away from the sensing surface and would be less likely to be detected.

One approach to avoiding the distorted U-shaped interface is to operate the flow focusing channel at as low a  $Re$  as possible. The simplest way to reduce  $Re$  is to reduce the flow rates. However, decreasing the  $Re$  by decreasing the flow rates increases the time for diffusion across the fluid boundary interface between the focused and focusing streams. This is particularly problematic where the function of the microfluidic system is inherently dependent on strict segregation of the fluid constituents. A way to decrease the  $Re$  while limiting diffusion is to use higher viscosity fluids. However, care must be taken to ensure that the viscosities are closely matched since a mismatch causes instabilities at the boundary between the two streams and results in unexpected focusing or even mixing behavior. Increasing viscosity can also have a negative impact on performance in sensor systems in terms of target transport to surfaces, conductivity measurements, or a need for more powerful pumps.

An alternative to decreasing flow rates or increasing viscosity to decrease  $Re$  is to manipulate the junction angle between the merging streams [9]. If the focusing stream intersects the focused stream at a very shallow angle, the focused stream exhibits a flatter profile than if the focusing stream is introduced perpendicular to the main channel (Figure

2). At steep junctions (e.g. T-junction), the velocity component of the focusing stream perpendicular to the main channel is maximized. The impact of the focusing stream momentum, which is strongest in the center due to the Poiseuille flow profile, is magnified. If perpendicular intersections are unavoidable, then a flatter profile for the focused stream can be obtained if the slower flowing stream, instead of the focusing stream, is introduced perpendicular to the main channel (Figure 3).

These inertial influences primarily exert an impact on the shape of the focused stream at the point where the inlets meet. Once the flow is fully developed in the main channel, further aberrations in most channels are primarily due to predictable Poiseuille velocity distributions. However, the main channel does not have to maintain a constant perimeter shape: fine control of the fluid positions in a microchannel can be achieved using grooves manufactured in the walls of the channel. We define such “grooves” to be either trenches or ridges and to include virtually any variety of shapes, though the shapes studied to date are primarily straight lines, chevrons, or herringbones. Groove features were originally introduced in microchannels to effect mixing, as in Stroock et al [1]. However, Mott et al. [11] found that since the grooves perform fluid advection in a predictable way, different groove shapes can be combined to achieve a desired remapping of the fluid in the channel cross-section. Stokes flow for each kind of groove feature was calculated and distilled into an advection map, which describes how all points in the channel cross-section are repositioned as the fluid is diverted by groove structures in the channel wall. Figure 4a shows how the distribution of two flows input into a channel side-by-side are modified by the advection caused by a single linear groove on one side of the microchannel. The effect of multiple groove features combine in a linear fashion; thus software was generated that quickly calculates the combination of the advection maps to predict the cross-sectional geometries for multiple streams within the channel after passing through the grooved region [12]. This Tiny Toolbox software calculates any combination of groove features much faster than computational fluid dynamic calculations. Figure 4b shows a set of groove features used to produce a passive microfluidic mixer, and illustrates not only the potential degree of complexity of the simulations but also the degree of agreement between the calculated (Figure 4c) and actual (Figure 4d) cross-sectional geometries of the flow streams within the microfluidic channel.

In the mixer example, fluids were introduced at equivalent flow rates. As an example of hydrodynamic focusing using grooves, Howell et al. [13] used Tiny Toolbox to predict two groove designs that transform focusing and focused fluids initially flowing side-by-side into fully sheathed flow, in which the “core” stream flows in the middle of the channel and is fully surrounded by the focusing “sheath” fluid. Either straight or chevron grooves were used in the top and bottom of the channel to redirect the focusing fluid above and below the slower flowing stream to compress it into the center of the channel. In addition to focusing the core in the center of the channel, the cross-sectional area was defined by the relative flow rates of the focused core and focusing streams.

In the examples following this section, we will illustrate how to control the impact of inertial effects at the inlets and to use advection controlled by grooves in the main channel to create a focused flow stream with a desired cross-sectional shape. We have selected three examples of very different applications to illustrate the impact of the principles on device design.

## Hydrodynamic focusing for impedance-based microfluidic biosensors

Detection sensitivity in impedance (or conversely, conductance)-based microfluidic biosensors is influenced by the dimensions of the microchannel. In order to attain maximum sensitivity (often defined as a percent change in impedance,  $\Delta R/R$ ) for such devices, it is

important that the microchannel have dimensions (simplified as cross-sectional area) comparable to those of the biological cell(s) to be detected. Gawad and colleagues [14], presented a general equation to describe the relationship between impedance change,  $\Delta R$ , and the ratio of a spherical particle's radius to microchannel cross-sectional area for Coulter counter devices. Theoretical resistance changes associated with the presence of a spherical particle within a microchannel can be determined using the following equation [14,15]:

$$\Delta R = 2\rho_{sol} \left[ \frac{\arctan\left(\frac{r_p}{\sqrt{A_c/\pi - r_p^2}}\right)}{\pi \sqrt{A_c/\pi - r_p^2}} - \frac{r_p}{A_c} \right] \quad (1)$$

where  $\Delta R$  is the change in impedance,  $r_p$  is the radius of the spherical particle,  $A_c$  is the cross-sectional area of the channel and  $\rho_{sol}$  is the solution conductivity. This equation was first presented in the book *Microfluidic Technology and Applications* by Koch et al. [15] and variations of this equation can be found elsewhere [16]. As the ratio of particle radius to cross-sectional area increases, the change in impedance,  $\Delta R$ , also increases and consequently, sensitivity increases.

The disadvantage of reducing the dimensions of a microchannel is the greater propensity for clogging when real-world samples are introduced. The use of a faster focusing stream to confine a stream of relatively slower flow rate to a narrow layer at the sensing surface was first described by Manz [17] as a way to use relatively large channels that are minimally susceptible to clogging. Hydrodynamic focusing of a conductive fluid has been used to make impedance-based microfluidic Coulter counters [18–20]. To decrease the likelihood of clogging, confinement of the electric current path can be achieved using hydrodynamic focusing, where the cross-sectional area defined in Equation 1 is not bounded by the physical dimensions of the microfluidic channel, but rather by the well-defined interface between the two fluid streams formed during laminar flow. When a high conductivity fluid is simultaneously introduced with a lower conductivity focusing fluid into a microchannel, the fractional volume occupied by the conducting fluid can be controlled by varying the ratio of the flow rate of the focusing fluid to that of the conducting fluid. Decreasing the volume of the channel occupied by the focused stream decreases its cross-sectional area, and consequently, the current can be confined to enhance the impedance change (according to Equation 1) in the presence of an insulating particle of defined radius. In essence, a virtual microchannel with pliable boundaries is created as a result of focusing the flow of the conducting fluid within the physical confines of the larger microfluidic channel. The ability to detect immobilized magnetic beads [10] and antibody-bound bacteria [21] has been demonstrated using hydrodynamic focusing in a four-electrode impedance-based microfluidic device.

The shape of the virtual conducting channel created by hydrodynamic focusing is important for achieving good sensitivity and is influenced by the flow-rate ratio of the focusing and conducting streams, as well as by the microfluidic channel geometry. Initially, Nasir and colleagues proposed a simple two-inlet T-junction design, where the focusing fluid inlet was perpendicular to both the conducting fluid inlet and the main microchannel containing coplanar electrodes for impedance measurements [10]. The result of this design was a focused stream with a U-shaped cross-sectional profile with cusps at the edges of the main channel (Figure 1). Increasing the flow-rate within the channel – necessary for increased focusing and current confinement – increased the height of the cusps. The disadvantage of the U-shaped profile was that the non-uniformity in the current density through the conducting focused stream concentrated the highest current density in the cusps and lowered

the current density at the center, where detection of immobilized cells and particles occurs. Decreasing the flow rate decreased the  $Re$ , making the focused layer more planar. However, the consequence of decreasing the flow rate was a larger cross-sectional area of the conducting path and lower sensitivity for detection of particles or cells. At the lower flow rates and  $Re$ , the rate of diffusion from the high conductivity focused stream to the focusing stream becomes an issue. To overcome the disadvantage presented by the cusp formation, Nasir and colleagues redesigned the device and created a sample inlet channel that was smaller in height and width than both the main channel and focusing fluid inlet [21]. The resulting focused stream had a dome-shaped profile that decreased in both height and width with increased focusing (Figure 5). The ability to confine both the height and width created a conducting fluid path with adjustable aperture for control over detection sensitivity for particles or cells captured between the electrodes.

Justin and colleagues [22] identified a number of additional factors, including ionic concentration and microchannel height, that also impact the response of impedance-based microfluidic devices employing hydrodynamic focusing. These factors must be taken into consideration when using such systems for cell detection. Ionic concentration can be affected by diffusion. Diffusion is not absent during focusing where both focusing and conducting fluids are aqueous; consequently, it is important to minimize the effects of ion loss from the conducting stream to the low conductivity focusing fluid. The rate of diffusion can be reduced by increasing the flow rates within the microchannel [21]. Two-phase systems would also effectively reduce diffusion; however, the difference in viscosities that often accompany two-phase systems can lead to instabilities at the interface that can adversely impact the impedance response. To overcome the issue of differential viscosities during flow focusing, Morgan's group used an oil/surfactant mixture (hexanediol containing 1% Tween 20) as the focusing fluid and phosphate buffered saline as the conducting fluid [23]. Another challenge identified by Justin and colleagues in using hydrodynamic focusing for impedance measurements was the noise generated by pulsatile flow associated with the syringe pumps used. This noise became more and more pronounced at the higher flow-rate ratios, decreasing the sensitivity. Such problems could be mediated by using pneumatic pumps to reduce pulsation or control electrodes for signal normalization. This also highlights the care that must be taken in the design of the microfluidic channels such that the focusing can be achieved with as few inlet channels (with different flow rates) as possible.

Using two inlets for focusing fluid on both sides of the channel, the conducting fluid can be focused not only over the electrodes on the bottom surface, but also laterally, producing a narrow rectangular focused stream hugging the bottom surface. By adjusting the relative flow rates of the side inlets, the conducting fluid stream can be swept across the bottom surface (e.g. between positive and negative control electrodes and assay electrodes or over sensor spots modified with different capture molecules). Figure 6a illustrates a four-inlet, single-outlet microfluidic device, with one inlet perpendicular to the main microchannel (for focusing the conducting fluid on the bottom of the channel), an inlet parallel to the channel (for the focused stream) and two side inlets at an angle of 45 degrees to the main channel (for side focusing streams). The top and side streams confine the focused stream in the vertical and lateral directions. In addition, by varying the flow-rate ratio of the side inlets with respect to each other, the focused stream can be swept from one side of the microchannel to the other with relatively high precision. In Figure 6b, confocal microscopy images of the cross-section of the main microchannel reveal the sweeping behavior of the focused stream from the right side to the left side of the channel achieved by varying the relative flow-rates of the side inlet fluids.

## Sheath flow for microflow cytometry

For accurate analysis of individual particles in a flow cytometer, the particles flow in a focused “core” stream surrounded by the “sheath” fluid that aligns the core within the interrogation optics. In conventional systems, concentric nozzles are used to inject a core stream in the middle of a sheath stream. However, a nozzle is difficult to fabricate and integrate into a microfluidic system. Howell, Ligler, and colleagues simplified previous microfluidic designs that required 3–4 inlets for focusing fluid to surround the core stream by placing grooves in the top and bottom of the channel to direct the sheath fluid completely around the core stream [24,25]. Initial groove designs used straight grooves that converted side-by-side core and sheath fluid into fully (360 degree) sheathed focused flow [13]. This design produced a central core where the diameter could be easily defined by the relative flow rates of the core and sheath streams; however, the lateral position of the core was susceptible to change caused by fluctuations in the pump introducing the sheath fluid. This problem was solved by splitting the sheath flow from a single pump into inputs on both sides of the core inlet and using chevron-shaped grooves to direct sheath fluid above and below the core. In this configuration, pulsation of the pump narrowed and widened the core but did not move it laterally in the channel. The chevron-based grooves were implemented in a flow cytometer system that used optical fibers to deliver the laser light and capture light scatter and fluorescence signals during the interrogation of color-coded microspheres [26,27]. Immunoassays have been performed using coded microspheres, demonstrating the ability to discriminate the microspheres and identify microspheres with captured target in multiplexed analyses that included simultaneous positive and negative internal controls. Sensitivity was equivalent to that obtained using a conventional nozzle-based flow cytometer. Channels manufactured using soft lithography are adequate for most applications, but they can swell and leak in systems that would require functioning in higher pressures. Thus this same chevron design was manufactured in hard plastic using a CNC mill [28]. Although the channel was slightly larger and the grooves had a more rounded shape due to the CNC milling, the device produced equivalent core focusing, and assays performed comparably with those conducted using the polydimethylsiloxane microflow cytometers.

By simply changing the excitation source and the emission filters, the same chevron groove design has been used to discriminate marine phytoplankton on the basis of light scatter as a rough measure of size and intrinsic fluorescence, primarily from chlorophyll and phycoerythrin [29,30]. The ability to have a very wide inlet, yet still focus individual cells within the laser beam using hydrodynamic focusing, meant that the cytometer could characterize phytoplankton ranging from *Synechococcus* with a diameter less than 1  $\mu\text{m}$  to *Pseudonitzschia*, a species as long as 80  $\mu\text{m}$ .

Hydrodynamic focusing with grooves in the top and bottom of the channel wall was used to solve another problem incurred as microflow cytometers are developed for use outside the laboratory. In certain environments, the requirement for large quantities of focusing fluid can be a significant logistical limitation. As long as the flow in a microfluidic system remains laminar, alterations in the flow path can be reversed. This condition is met in the microflow cytometer as hydrodynamic focusing using advection by grooves in the channel walls not only can focus the core stream using the sheath flow, but can also reverse the focusing, returning the core and sheath streams to their original positions [31]. As depicted in Figure 7, the grooves were reversed to “unsheathe” the core stream. To ensure clean separation and complete recovery of particles into the central outlet, under the flow conditions compatible with the cytometric analyses, only about 10% of the sheath fluid had to be sacrificed into the core stream. This process provides sheath fluid uncontaminated with sample for reuse and minimally diluted sample for further analysis. The reversibility of

hydrodynamic focusing has applications for automated processing of cells and particles, as well as for long-term unattended use of flow cytometers.

## Hydrodynamic shaping for microfabrication

Round fibers with micron and sub-micron diameters have been fabricated in microfluidic channels using hydrodynamic focusing [32–39]. Multiple annular flows were utilized by Lan et al. to fabricate 300–900  $\mu\text{m}$  tubes with adjustable wall thicknesses [40]. In addition to polymerization of fibers using chemical and UV initiators, rectangular fibers have been precipitated at the interface between two streams in a microfluidic channel; this approach, however, is limited in its ability to release the fibers from the channels [41–43].

The strategy of using advection maps derived from sets of grooves in the channel walls was employed to produce a design that can manipulate a focusing stream to shape a core stream into a pre-determined cross-sectional shape. An application that exploits this implementation of hydrodynamic focusing is the micromanufacture of polymer fibers with defined cross-sectional shapes and sizes (Figure 8). Both casting [44] and photopolymerization [45] were used to form non-round fibers from a prepolymer core shaped in a focusing stream directed by groove structures in the channel walls. Most fibers are round in shape due to surface tension in the two-phase systems (liquid/air; liquid/solid) in which they are produced. The sheathing of a prepolymer core with a focusing stream of the same phase provides the opportunity for creation of fibers with more complex shapes. Control of the relative flow rates of the focusing stream and the prepolymer core creates fibers with the desired cross-sectional area; this approach has been used to fabricate meters of fibers from 300 nm to 300  $\mu\text{m}$  across and even to alter the fiber diameter during the production process.

A wide variety of shapes and applications are conceivable. Howell et al. demonstrated that five streams could be sequentially introduced between groove sets so that each stream completely surrounded the streams introduced upstream [46]. Polymerization of such layers and other complex shapes offers intriguing possibilities. Continuous fabrication of particles and fibers could result in new materials for wound dressings, tissue regeneration, controlled release structures and environmentally responsive materials, or unique light-weight textiles.

## Conclusions

Hydrodynamic focusing is a versatile tool that can be used with microfluidic systems for applications as diverse as creating conducting microchannels with adjustable apertures for control over detection sensitivity to microfabrication of nano- to micro-scale polymer fibers with unique shapes and material properties. Research by our group in the area of hydrodynamic focusing has produced a toolbox strategy for using passive structures for advection-based control of a focused stream and has revealed that there is significant inertia even at low  $Re$  that can impact the shape of the focused stream. We have demonstrated a few of the methods by which hydrodynamic focusing can be used for precise positioning of cells, particles, sensor targets, molecular recognition elements or prepolymers through positioning of a focused stream containing such materials within a predetermined region of a microfluidic device. The list does not end here. Exciting possibilities for currently unexplored applications of hydrodynamic focusing await further research into the behavior of multiphase fluids within microchannels, the interaction of hydrodynamic forces with elements directed by optical, conducting, or magnetic forces, and further understanding of the subtle but critical changes dependent on microchannel geometry, flow parameters and fluid behavior.

## Acknowledgments

This work was funded by NRL/ONR WU 9899, NRL 6.2 Work Unit 6027 and the Defense Threat Reduction Agency. The views are those of the authors and do not represent the opinion or policy of the US Navy or the Department of Defense. The authors wish to thank Adam Shields and Abel Thangawng for the electron micrographs of the extruded polymer fibers. GJ is a National Research Council postdoctoral fellow.

## References

1. Stroock AD, Dertinger SKW, Ajdari A, Mezic I, Stone HA, Whitesides GM. *Science*. 2002; 295(5555):647–651. [PubMed: 11809963]
2. Osborn JL, Lutz B, Fu E, Kauffman P, Stevens DY, Yager P. *Lab Chip*. 2010; 10(20):2659–2665. [PubMed: 20680208]
3. Howell PB, Mott DR, Fertig S, Kaplan CR, Golden JP, Oran ES, Ligler FS. *Lab Chip*. 2005; 5(5): 524–530. [PubMed: 15856089]
4. Weigl BH, Yager P. *Science*. 1999; 283(5400):346–347.
5. Atencia J, Beebe DJ. *Nature*. 2005; 437(7059):648–655. [PubMed: 16193039]
6. Walsh PA, Walsh EJ, Davies MRD. *International J Heat Fluid Flow*. 2007; 28(1):44–53.
7. Lee GB, Chang CC, Huang SB, Yang RJ. *J Micromech Microengin*. 2006; 16(5):1024–1032.
8. Howell PB, Mott DR, Golden JP, Ligler FS. *Lab Chip*. 2004; 4(6):663–669. [PubMed: 15570382]
9. Nasir M, Mott D, Kennedy M, Golden J, Ligler F. *Microfluid Nanofluid*. 11(2):119–128.
10. Nasir M, Ateya DA, Burk D, Golden JP, Ligler FS. *Biosens Bioelectron*. 2010; 25(6):1363–1369. [PubMed: 19932019]
11. Mott DR, Howell PB, Golden JP, Kaplan CR, Ligler FS, Oran ES. *Lab Chip*. 2006; 6(4):540–549. [PubMed: 16572217]
12. Howell PB, Mott DR, Ligler FS, Golden JP, Kaplan CR, Oran ES. *J Micromech Microeng*. 2008; 18(11):115019(1)–115019(7).
13. Howell PB, Golden JP, Hilliard LR, Erickson JS, Mott DR, Ligler FS. *Lab Chip*. 2008; 8(7):1097–1103. [PubMed: 18584084]
14. Gawad S, Schild L, Renaud P. *Lab Chip*. 2001; 1(1):76–82. [PubMed: 15100895]
15. Koch, M.; Evans, A.; Brunnschweiler, A. *Microfluidic Technology and Applications*. Hertfordshire, England: Research Studies Press Ltd.; 2000. 320 p.
16. Nieuwenhuis JH, Kohl F, Bastemeijer J, Sarro PM, Vellekoop MJ. *Sens Act B: Chemical*. 2004; 102(1):44–50.
17. Hofmann O, Voirin G, Niedermann P, Manz A. *AnalChem*. 2002; 74(20):5243–5250.
18. Blankenstein G, Larsen UD. *Biosens Bioelectron*. 1998; 13(3–4):427–438.
19. Simonnet C, Groisman A. *AnalChem*. 2006; 78(16):5653–5663.
20. Rodriguez-Trujillo R, Castillo-Fernandez O, Garrido M, Arundell M, Valencia A, Gomila G. *BiosensBioelectron*. 2008; 24(2):290–296.
21. Nasir M, Price DT, Shriver-Lake LC, Ligler F. *Lab Chip*. 2010; 10(20):2787–2795. [PubMed: 20725680]
22. Justin G, Nasir M, Ligler FS. *Anal Bioanal Chem*. 2011; 400(5):1347–1358. [PubMed: 21448604]
23. Bernabini C, Holmes D, Morgan H. *Lab Chip*. 2011; 11(3):407–412. [PubMed: 21060945]
24. Ateya DA, Erickson JS, Howell PB, Hilliard LR, Golden JP, Ligler FS. *Anal Bioanal Chem*. 2008; 391(5):1485–1498. [PubMed: 18228010]
25. Ligler, FS.; Kim, JS. *The Microflow Cytometer*. Pan Stanford Publishing;
26. Golden JP, Kim JS, Erickson JS, Hilliard LR, Howell PB, Anderson GP, Nasir M, Ligler FS. *Lab Chip*. 2009; 9(13):1942–1950. [PubMed: 19532970]
27. Kim JS, Anderson GP, Erickson JS, Golden JP, Nasir M, Ligler FS. *Anal Chem*. 2009; 81(13): 5426–5432. [PubMed: 19496600]
28. Thangawng AL, Kim JS, Golden JP, Anderson GP, Robertson KL, Low V, Ligler FS. *Anal BioanalChem*. 2010; 398(5):1871–1881.



29. Hashemi N, Erickson JS, Golden JP, Jackson KM, Ligler FS. *Biosens Bioelectron.* 26(11):4263–4269. [PubMed: 21601442]
30. Hashemi N, Erickson JS, Golden JP, Ligler F. *Biomicrofluidics.* 2011; 5(3)
31. Hashemi N, Howell PB, Erickson JS, Golden JP, Ligler FS. *Lab Chip.* 2010; 10(15):1952–1959. [PubMed: 20480064]
32. Shapiro, E.; Drikakis, D.; Gargiuli, J.; Vadgama, P. *Proceedings of the 4th International Conference on Nanochannels, Microchannels, and Minichannels, Pts A and B; 2006.* p. 829-836.
33. Chang CC, Huang ZX, Yang RJ. *J Micromech Microengin.* 2007; 17(8):1479–1486.
34. Ohm C, Serra C, Zentel R. *Adva Materials.* 2009; 21(47):4859–4863.
35. Jeong W, Kim J, Kim S, Lee S, Mensing G, Beebe DJ. *Lab Chip.* 2004; 4(6):576–580. [PubMed: 15570368]
36. Jeong, WJ.; Mensing, G.; Lee, SH.; Beebe, DJ. *Micro Total Analysis Systems 2004.* Laurell, T.; Nilsson, J.; Jensen, K.; Harrison, DJ., editors. Vol. Vol 2. Royal Society of Chemistry Special Publications; 2005. p. 533-535.
37. Jo E, Lee SW, Kim KT, Won YS, Kim HS, Cho EC, Jeong U. *Adv Materials.* 2009; 21(9):968–972.
38. Marimuthu M, Kim S. *An J Soft Matter.* 2010; 6(10):2200–2207.
39. Kang E, Shin SJ, Lee KH, Lee SH. *Lab Chip.* 10(14):1856–1861. [PubMed: 20454720]
40. Lan WJ, Li SW, Lu YC, Xu JH, Luo GS. *Lab Chip.* 2009; 9(22):3282–3288. [PubMed: 19865737]
41. Hou S, Wang S, Yu ZTF, Zhu NQM, Liu K, Sun J, Lin WY, Shen CKF, Fang X, Tseng HR. *Angewandte Chemie-Int Ed.* 2008; 47(6):1072–1075.
42. Steinbacher JL, McQuade DT. *J Polymer Sci A-Polymer Chemistry.* 2006; 44(22):6505–6533.
43. Kenis PJA, Ismagilov RF, Whitesides GM. *Science.* 1999; 285(5424):83–85. [PubMed: 10390366]
44. Thangawng AL, Howell PB, Richards JJ, Erickson JS, Ligler FS. *Lab Chip.* 2009; 9(21):3126–3130. [PubMed: 19823729]
45. Thangawng AL, Howell PB, Spillmann CM, Naciri J, Ligler FS. *Lab Chip.* 2011; 11(6):1157–1160. [PubMed: 21246152]
46. Mott D, Howell PB, Ligler FS, Fertig S, Bobrowski A. *Sheath flow device and method.* US2009208372-A1. 2009
47. Nasir, M.; Ligler, F. *Technical Digest of MicroTAS, the 15th International Conference on Miniaturized Systems for Chemistry and Life Sciences; Seattle, Washington.* 2011.

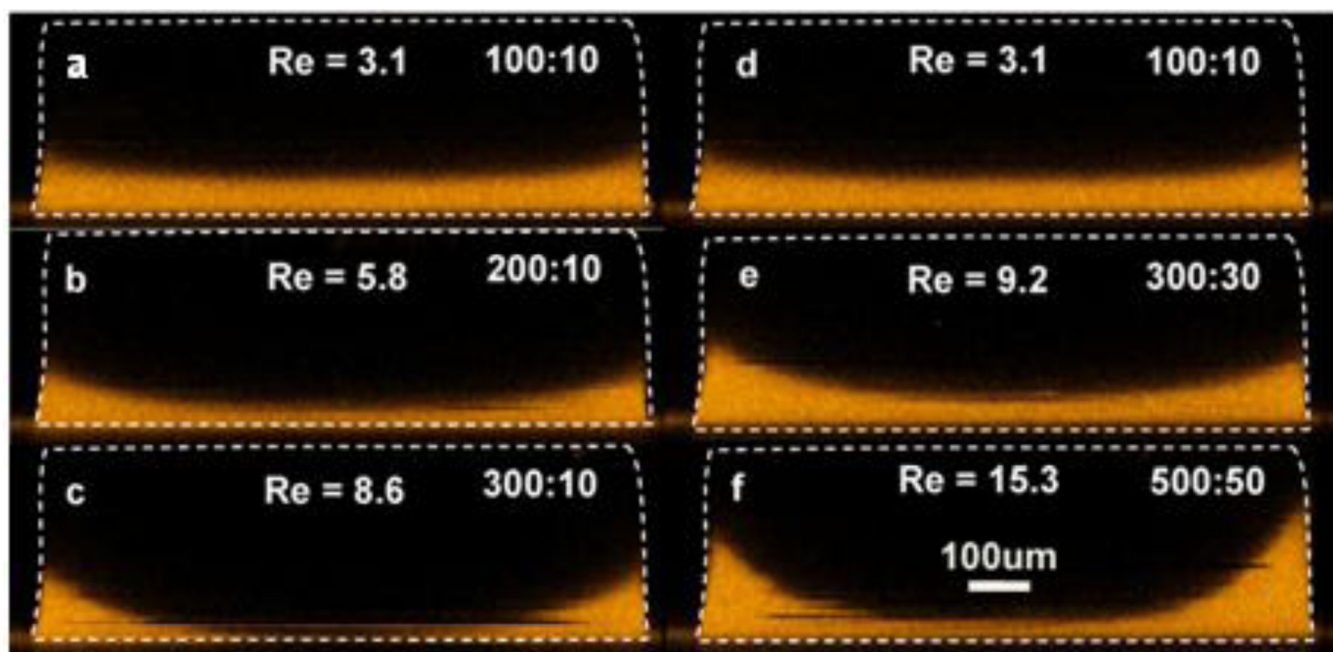


**Figure 1.** This series of confocal images shows the effects of increasing flow-rate ratio (a–c) and increasing the Re while maintaining the flow-rate ratio of 10 (d–f) on the concentration profile of the focused stream. The fluid viscosity and density were respectively  $1 \times 10^{-3}$  Pa·s and  $1 \times 10^3$  kg/m<sup>3</sup> for all tests. Re numbers were calculated based on the channel dimensions and the flow rates. Numbers in the top right of each image indicate the flow rates for the focusing and focused streams in  $\mu\text{L}/\text{min}$  [10]

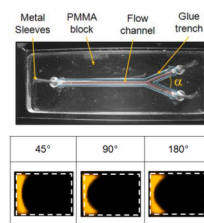


**Figure 2.**

Microchannels were fabricated from polymethylmethacrylate (PMMA) and attached to a glass slide using UV-curable glue. A trench around the boundary of the main channel prevented the glue from running into the channel. All channels were 600  $\mu\text{m}$  wide and 400  $\mu\text{m}$  deep ( $\pm 10\mu\text{m}$ ). Confocal cross-sectional images of the main channel show the focused region for three angles of confluence ( $\alpha$ ). Flow rates for the sheath and focused streams were 720 and 29  $\mu\text{L}/\text{min}$ , respectively ( $\text{Re} \approx 25$ ). Deionized water was used for both streams with rhodamine dye added to the focused stream only [47]

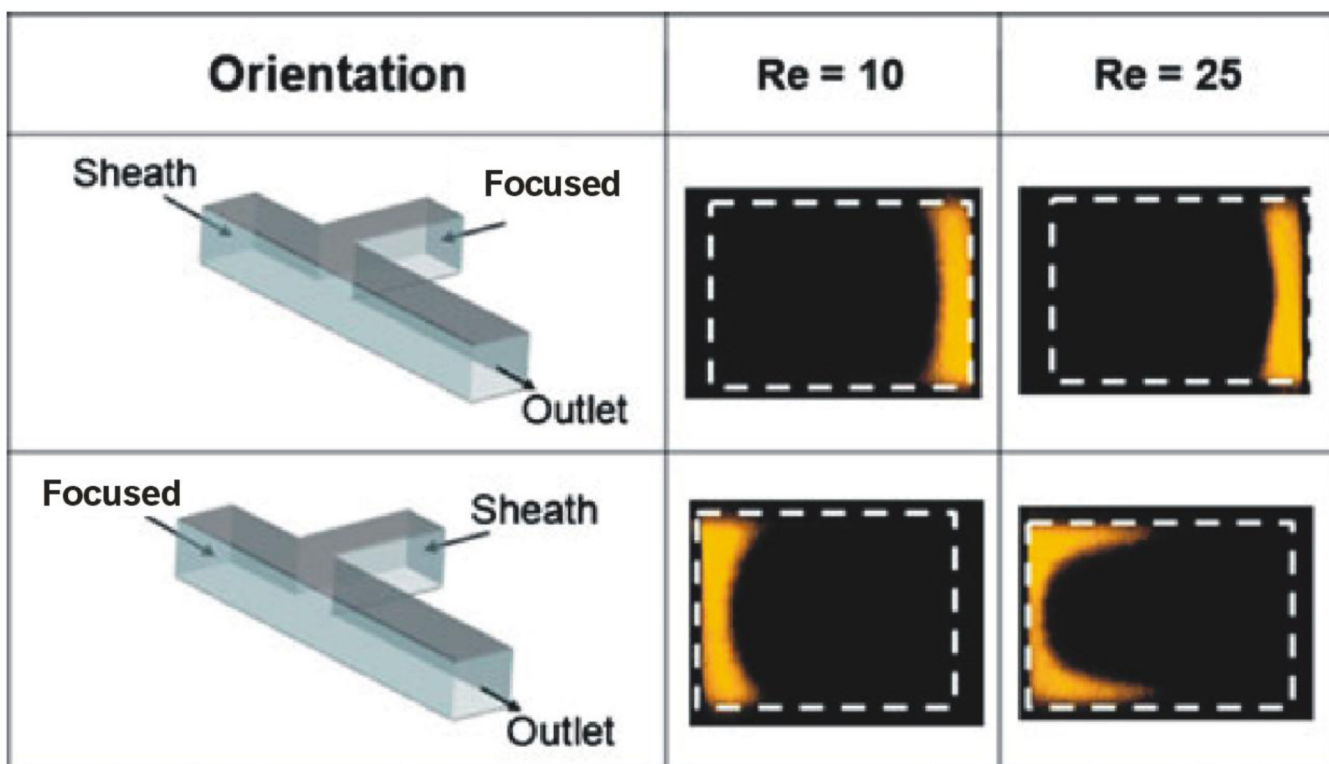


**Figure 3.**

Channel cross-sectional images from confocal microscopy show the concentration profiles for a conventional T-inlet channel design ( $\alpha = 90^\circ$ ). The sheath and focused streams were switched for each case of the Re (10, 25). The first row shows the case in which the sheath stream was aligned with the main channel. The second row shows the results in which the focused stream was aligned with the main channel. The channel was  $380 \mu\text{m} \times 600 \mu\text{m}$  (height  $\times$  width). The flow rates for the focused stream and sheath flow, respectively, were 11 and  $283 \mu\text{L}/\text{min}$  for  $\text{Re} \approx 10$  and 28 and  $707 \mu\text{L}/\text{min}$  for  $\text{Re} \approx 25$  [9]

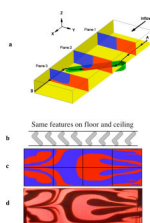


**Figure 4.** Tiny Toolbox uses combinations of advection maps to predict what grooved structures will produce desired interactions of multiple laminar flow streams. a) flow path of a single particle through a groove b) groove structures to achieve complex fluid interfaces for mixing purposes c) simulations of the outflow patterns using Tiny Toolbox, d) confocal images of flow in actual channel using the specified grooves [11]

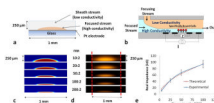


**Figure 5.**

Hydrodynamic focusing to confine a conducting stream. a) Microchannel cross-section indicating the focused stream over a platinum electrode on glass slide. b) Partial side view of microchannel (not drawn to scale) indicating direction of sheath, sample, and outlet flows during hydrodynamic focusing. Flow focusing is used to increase sensitivity to specifically bound cells or particles between the impedance sensing electrodes. c) Finite element analysis simulations in COMSOL of flow-rate ratios. d) Confocal microscopy images of sample stream (water with rhodamine dye) under varying flow-rate ratios (in  $\mu\text{L}/\text{min}$ ). e) Theoretical and experimental impedance change with increased focusing [22]

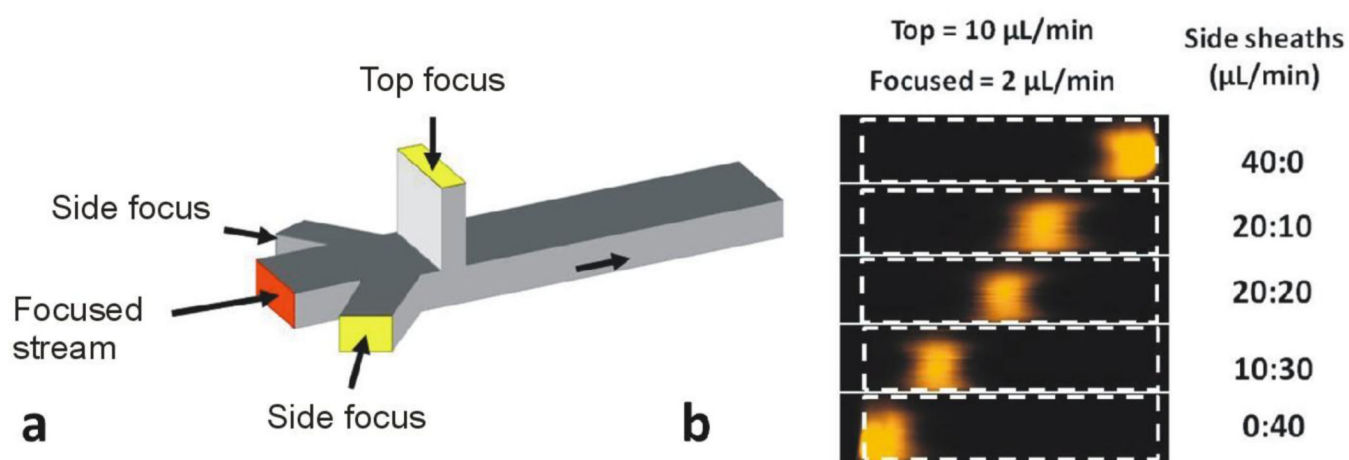


**Figure 6.** Use of hydrodynamic focusing to move a focused stream during operation of a microfluidic device. a) Illustration of a four-inlet microfluidic device with three focusing fluid inlets and a single focused stream inlet. b) Confocal microscopy images of the focused stream (visualized using a rhodamine dye) during a side-to-side focusing operation. Flow rates of the left and right side focusing streams are indicated to the right of Figure 6b

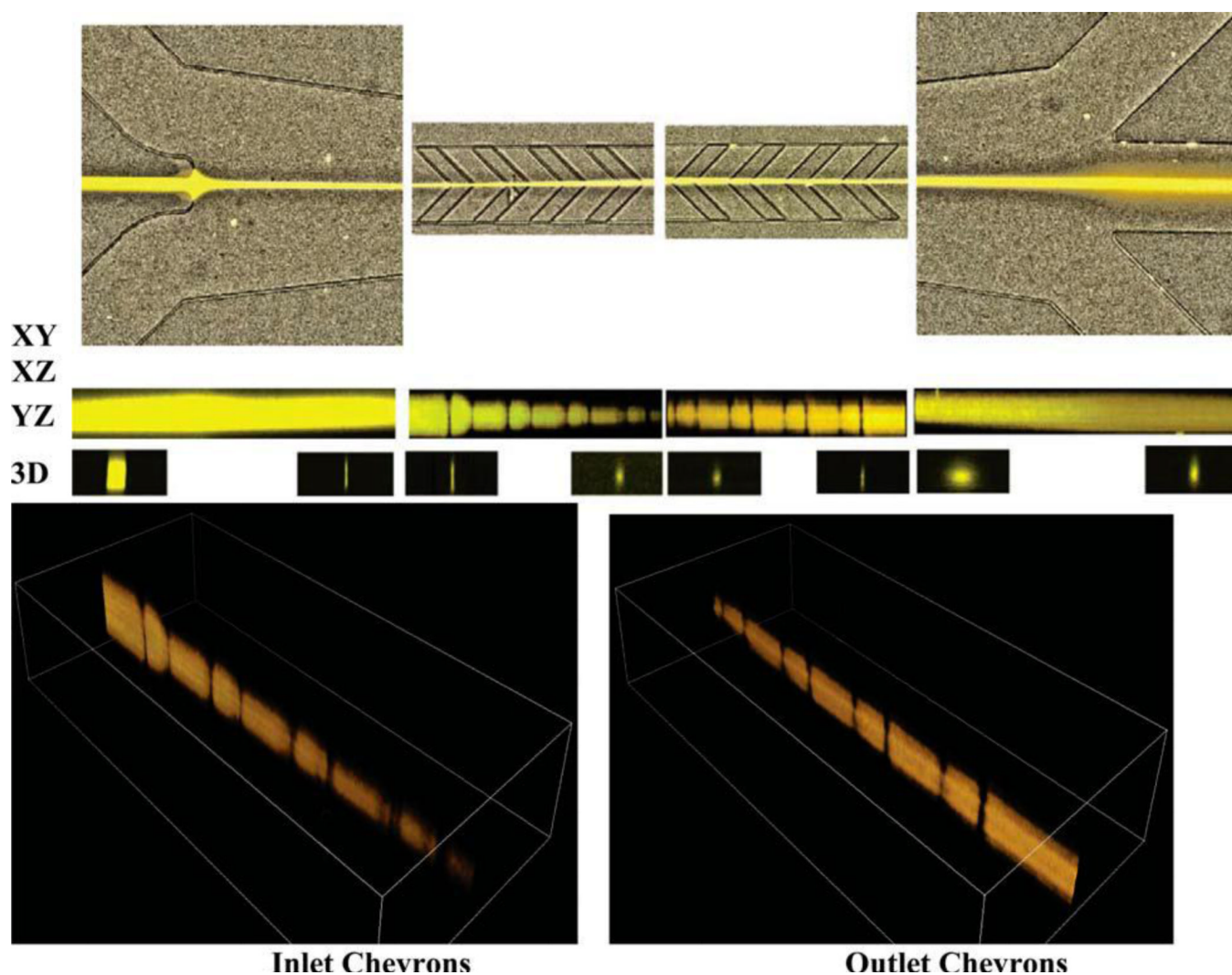


**Figure 7.** Confocal microscopy images of the sheathing and unsheathing processes at 90% sheath fluid recycling. XY: top view of the inlet, inlet chevrons, reverse chevrons, and outlet sections of the microchannel. XZ: side view of the same sections. YZ: cross-section views at upstream and downstream edges of each of the sections in the XY and XZ panels directly above. 3D: constructed images of the sample fluid at the inlet and reverse chevrons. The sample stream height decreases upon passing through the inlet chevrons and increases by passing through each reverse chevron. The inlet sample flow rate is 10  $\mu\text{L}/\text{min}$  and the sheath flow rate is 1100  $\mu\text{L}/\text{min}$ . The outlet sample flow rate is 120  $\mu\text{L}/\text{min}$  [31]



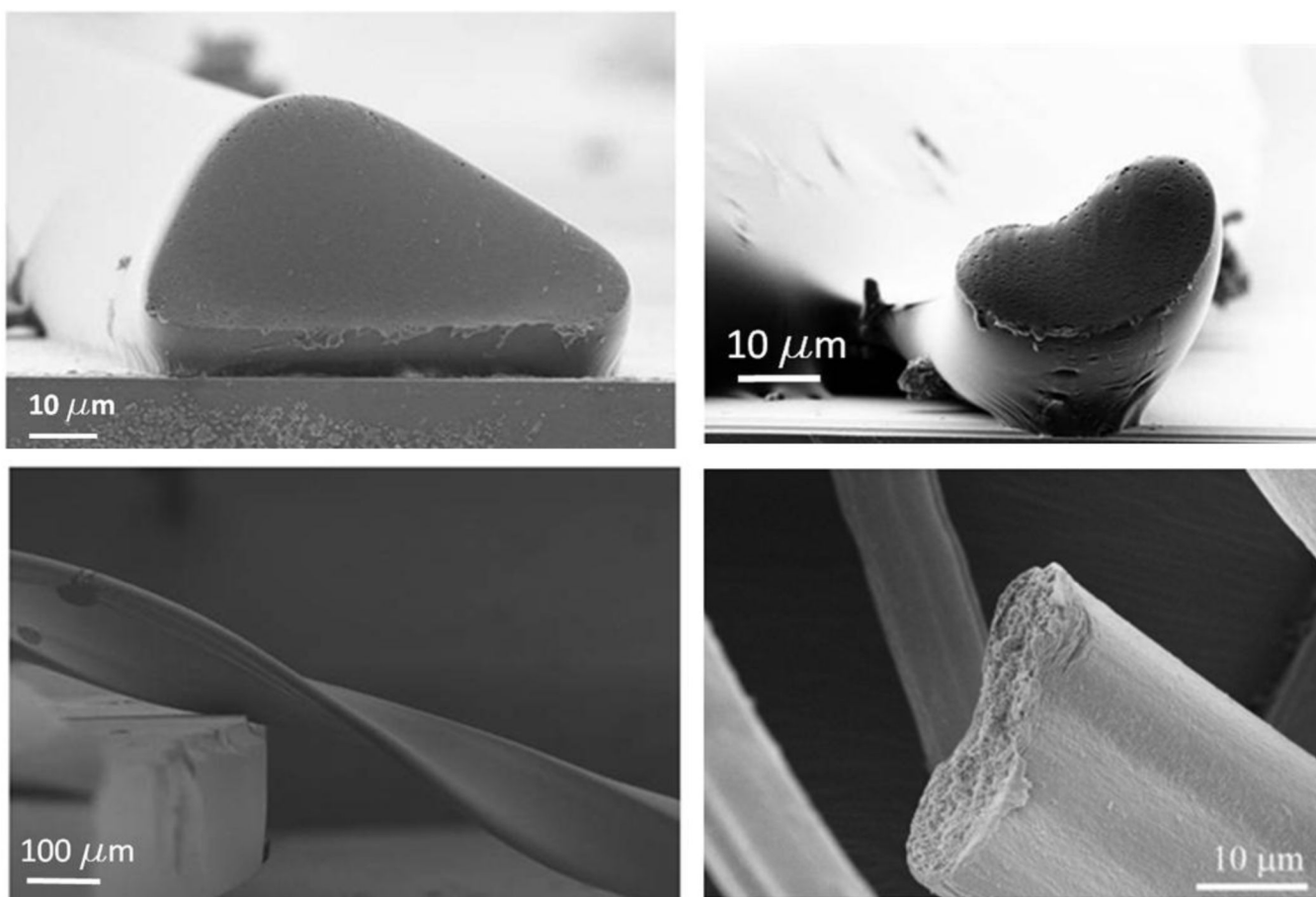


**Figure 8.** Scanning electron microscope images of polymer fibers micromanufactured using hydrodynamic focusing to control shape and cross-sectional area